

Individualized Multi-Treatment Response Curves Estimation using RBF-net with Shared Neurons

PETER CHANG, ARKAPRAVA ROY

Department of Biostatistics, University of Florida, United States

pchang27@ufl.edu, arkaprava.roy@ufl.edu

February 9, 2024

Abstract

Heterogeneous treatment effect estimation is an important problem in precision medicine. Specific interests lie in identifying the differential effect of different treatments based on some external covariates. We propose a novel non-parametric treatment effect estimation method in a multi-treatment setting. Our non-parametric modeling of the response curves relies on radial basis function (RBF)-nets with shared hidden neurons. Our model thus facilitates modeling commonality among the treatment outcomes. The estimation and inference schemes are developed under a Bayesian framework using thresholded best linear projections and implemented via an efficient Markov chain Monte Carlo algorithm, appropriately accommodating uncertainty in all aspects of the analysis. The numerical performance of the method is demonstrated through simulation experiments. Applying our proposed method to MIMIC data, we obtain several interesting findings related to the impact of different treatment strategies on the length of ICU stay and 12-hour SOFA score for sepsis patients who are home-discharged.

Keywords: Bayesian; ICU; MIMIC data; Multi-treatment regime; Radial basis network; Treatment effect.

1 Introduction

Estimation of heterogeneous treatment effects from observational data has become an important problem. It plays a crucial role in determining the individualized causal effects of a treatment, which then leads to a personalized assignment of optimal treatment (Wendling et al., 2018; Rekkas et al., 2020). Estimation of such heterogeneity however requires reasonable representations from each treatment subgroup. With the increasing availability of large-scale health outcome data such as electronic health records (EHR) data in recent years, it has become possible to develop individualized treatment strategies efficiently. This led to the development of several novel statistical methods, primarily tailored for binary treatment scenarios (Wendling et al., 2018; Cheng et al., 2020), with some accommodating multiple treatment settings (Brown et al., 2020; Chalkou et al., 2021). Most of these approaches are specifically designed for estimating population average treatment effects (ATEs) (Van Der Laan and Rubin, 2006; Chernozhukov et al., 2018; McCaffrey et al., 2013) and more recently, methods are being developed to estimate conditional average treatment effects (CATEs) (Taddy et al., 2016; Wager and Athey, 2018; Künzel et al., 2019; Nie and Wager, 2021). Here, we tackle a generic problem of heterogeneous treatment effect or CATE estimation in a multi-treatment setting, where the treatment responses may share some commonalities.

In the binary treatment setting, to estimate the treatment effect $\tau(\mathbf{x})$ in terms of a function of the predictor vector \mathbf{x} , one may start with a mean-zero additive error representation of a continuous treatment outcome y_i as $y_i = f(\mathbf{x}_i, z_i) + \epsilon_i$, where z_i is a treatment indicator for the i -th subject. Under this model, $\tau(\mathbf{x}_i) = f(\mathbf{x}_i, 1) - f(\mathbf{x}_i, 0)$ or $f(\mathbf{x}_i, z_i) = \mu(\mathbf{x}_i) + \tau(\mathbf{x}_i)z_i$ (Hahn et al., 2020) can be used for a direct estimation of the treatment effect. Alternatively, one may model each treatment group separately with two functions $f_0(\mathbf{x}_i)$ and $f_1(\mathbf{x}_i)$ and define $\tau(\mathbf{x}_i) = f_1(\mathbf{x}_i) - f_0(\mathbf{x}_i)$. These two approaches are known as S-learner and T-learner, respectively (Künzel et al., 2019). In addition, Künzel et al. (2019) proposes the X-learner approach for CATE estimation. Specifically, on Bayesian causal inference, Li, Ding and Mealli (2023) provides a critical review of this topic. Estimation of heterogeneous treatment effect is closely related to the problem of learning optimal treatment regimes, which has vast literature (Zhang et al., 2012; Luedtke and Van Der Laan, 2016; Jiang et al., 2017; Cui and Tchetgen Tchetgen, 2021) and more references can be found in this recently published review paper Li, Chen, Laber, Liu and Baumgartner (2023).

To model the outcome in a multi-treatment setting, one may either set treatment-specific functions as in the T-learner setting or develop a model with the treatment indicator as a predictor as in S-learning. Our approach to multi-treatment effect estimation is somewhat similar to T-learner, which relies on specifying treatment-specific outcome functions. However, traditional T-learners do not work very well when a common behavior is expected to appear in the two response functions, as shown in Künzel et al. (2019) for a two-treatment design. This motivated us to propose a model that directly allows the outcome functions to share some intrinsic characteristics.

Specifically, we propose a radial basis functions-based modeling approach for the unknown outcome functions with shared and treatment-group-specific neurons, accommodating both similarities and variations in the underlying treatment outcomes. In ICU data, such as MIMIC, there are often instances where two or three drugs are administered simultaneously. For example, in the MIMIC application, patients with sepsis often receive treatments such as mechanical ventilation (Peine et al., 2021; Zhu et al., 2021; Hu et al., 2021), vasopressor (Hu et al., 2021; Xu et al., 2023; He et al., 2023), or even a combination of those. Then the vitals or other clinical outcomes under these different treatment strategies could exhibit some shared characteristics. In clinical trials, too, investigators frequently structure trial arms in a way that involves multiple arms sharing a common drug (James et al., 2016; Ursprung et al., 2021). Thus, in the treatment effects of different trial arms, there may be some commonalities. Our modeling approach draws inspiration from these scenarios. Furthermore, the underlying mechanisms of several treatments often share common pathways, which may be reflected in the estimated treatment effects (Jones et al., 2003; White et al., 2011). More generally, it is possible to employ our proposed modeling framework to estimate the mean functions in a multi-group setting, where the outcome functions are anticipated to exhibit shared features.

We further propose a thresholding-based inference procedure relying on the best linear projections from Cui et al. (2023). Specifically, we first modify the approach from Cui et al. (2023) for inference using the posterior samples and then propose a variable importance estimation procedure by combining a thresholding step. The estimated importance values are shown to work reasonably well in simulation and are later used for inference in our MIMIC application.

The remainder of this article is organized as follows. The subsequent section introduces our proposed modeling framework. Section 3.1 discusses our Bayesian inference scheme detailing the prior

specification, likelihood computation, detailed posterior computation steps, and linear projection-based inference scheme. Subsequently, in Section 4, we analyze and compare the effectiveness of our proposed method against other competing approaches under various simulation settings. Finally, we apply our proposed method to study the effect of different treatments on patients, who suffered from acute sepsis and were discharged to home at the end of their ICU visit using MIMIC data in Section 5, and Section 6 is dedicated to discussing the overall conclusion and potential extensions.

2 Model

We consider G treatments and assume that there are P covariates. Let y_i be a continuous treatment outcome for the i -th patient with subject-specific P -dimensional covariates specified by \mathbf{x}_i . Then, our model for y_i when treated under the g -th treatment is,

$$\begin{aligned}
 y_i &= f_g(\mathbf{x}_i) + \epsilon_i, \\
 \epsilon_i &\sim \text{Normal}(0, \sigma^2), \\
 f_g(\mathbf{x}_i) &= \alpha + \sum_{k=1}^K \gamma_{k,g} \theta_k \exp\{-(\mathbf{x}_i - \boldsymbol{\mu}_k)^T (\mathbf{x}_i - \boldsymbol{\mu}_k) / b_k^2\}.
 \end{aligned} \tag{1}$$

Here, $f_1(\cdot), \dots, f_G(\cdot)$ denote the treatment-specific outcome functions modeled using a common set of radial basis function (RBF) neurons. Each function has a treatment-specific parameter $\boldsymbol{\gamma}_g = (\gamma_{k,g})_{1 \leq k \leq K}$ in its coefficients, where $\gamma_{k,g} \in \{0, 1\}$, and $\boldsymbol{\mu}_k, \theta_k \in \mathbb{R}$. We then construct the parameter $\boldsymbol{\Gamma} = ((\gamma_{k,g}))_{1 \leq k \leq K, 1 \leq g \leq G}$ as a $K \times G$ dimensional binary matrix. This matrix plays a crucial role in our proposed model, controlling the set of RBF bases to be used in specifying a treatment-specific outcome function. Specifically, $\gamma_{k,g}$ is 1 whenever the k -th RBF basis is included in modeling $f_g(\mathbf{x})$. A schematic representation of the proposed mode is in Figure 1.

In our modeling framework, although $\boldsymbol{\Gamma}$ controls shared and treatment-specific RBF bases, we are not specifically interested in identifying similarities in the response functions using this parameter. Our proposed model falls under the class of T-learner type models, which are often inefficient in estimating the treatment-specific functions sharing a common behavior, as pointed out in Künzel et al. (2019). The role of $\boldsymbol{\Gamma}$ is to address this inefficiency, alleviate this drawback, and help in estimating the outcome functions that may share some common characteristics.

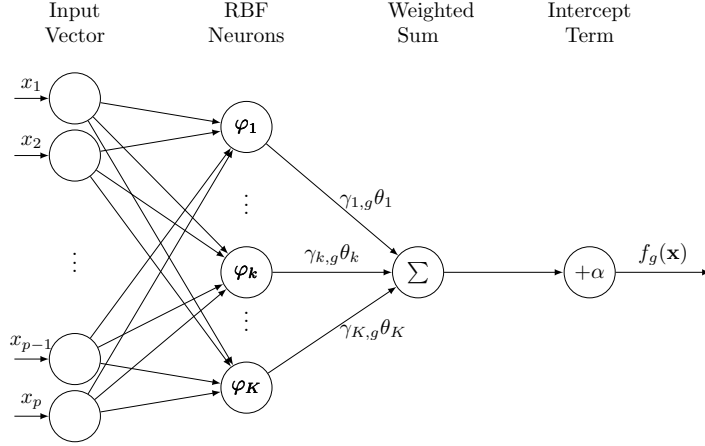


Figure 1: A schematic representation of our proposed RBF-net where $\varphi_k(x) = \exp\{-\frac{(\mathbf{x}_i - \boldsymbol{\mu}_k)^T(\mathbf{x}_i - \boldsymbol{\mu}_k)}{b_k^2}\}$. The activation functions are varying at each hidden unit due to the different centers $\boldsymbol{\mu}_k$. The $\gamma_{k,g}$'s are binary and control the inclusion of the neurons.

In our proposed model, the conditional treatment effect of g over g' for an array of covariates \mathbf{x} is identified as $\tau_{gg'} = f_g(\mathbf{x}) - f_{g'}(\mathbf{x})$ under assumptions that 1) given \mathbf{x} , treatment assignments are random and do not depend on the outcome, 2) the overlap condition $1 > P(z_i = g | \mathbf{x}_i) > 0$ holds for all i , where z_i is the treatment assignment variable such that $z_i = g$ implies i -th subject is treated under g -th treatment and 3) standard stable unit treatment value assumption (SUTVA) is maintained requiring no interference that one subject's potential outcomes are not affected by other subjects' treatment assignments.

3 Bayesian inference

We pursue a Bayesian approach to carry out the inference of the proposed RBF-net model with shared neurons, aiming to automatically quantify estimation uncertainty. In our model, $\{\Gamma, \boldsymbol{\mu}, \alpha, \boldsymbol{\theta}, \sigma, K\}$ is the complete set of parameters. Here, $\alpha \in \mathbb{R}$, $\sigma \in \mathbb{R}$, and $K \in \mathbb{R}$. As stated in Section 2, $\Gamma = ((\gamma_{k,g}))_{1 \leq k \leq K, 1 \leq g \leq G}$ is a $K \times G$ dimensional binary matrix. The RBF-centers $\boldsymbol{\mu} = \{\boldsymbol{\mu}_1, \dots, \boldsymbol{\mu}_K\}$ is $P \times K$ dimensional matrix, where $\boldsymbol{\mu}_k = ((\mu_{p,k}))_{1 \leq p \leq P}$. α is the intercept, $\boldsymbol{\theta} = \{\theta_1, \dots, \theta_K\}$ is the K -length vector of coefficients, σ is the error standard deviation, and finally K is the total number of RBF-bases. Although K is unknown, we first specify the priors and illustrate the posterior computation steps assuming a given value of K . In Section 3.4, our specification

procedure for K is discussed following an empirical Bayes-type strategy.

3.1 Prior specification

To proceed with our Bayesian analysis, we put prior distributions on the parameters. We assume independent priors for $\mathbf{\Gamma}, \boldsymbol{\mu}, \alpha, \boldsymbol{\theta}, \sigma$. They are described below in detail.

1. The basis inclusion indicators ($\mathbf{\Gamma}$): Following Kuo and Mallick (1998), each indicators are chosen independently with a Bernoulli distribution, $\gamma_{k,g} \sim \text{Bernoulli}(p_g)$ where $p_g \sim \text{Beta}(c, d)$.
2. The RBF-centers ($\boldsymbol{\mu}$): We put a multivariate normal distribution as the prior for $\boldsymbol{\mu}$, $\mu_{p,k} \sim \text{Normal}(0, \sigma_\mu^2)$.
3. The intercept and coefficients ($\alpha, \boldsymbol{\theta}$): We let both $\alpha, \theta_k \sim \text{Normal}(0, \sigma_d^2)$, with a pre-specified σ_d .
4. The error variance (σ): We specify a half-Cauchy prior for σ as $\sigma \sim C^+(0, \hat{\sigma})$.

Details for the specifications of c , d , σ_μ , and σ_d is given in Section 3.5. The choice of the half-Cauchy distribution as prior for σ is motivated by Linero and Yang (2018). We set $\hat{\sigma}$ to be the error standard deviation from the linear regression model, where the outcome is regressed on the predictors and the treatment covariate as a factor.

3.2 Likelihood function of data

In this section, we formalize the posterior likelihood function for our Bayesian inference model, considering both the observed data and the relevant parameters. The likelihood of our proposed model is

$$p(\mathbf{y}|\mathbf{\Gamma}, \boldsymbol{\mu}, \boldsymbol{\theta}, \alpha, \sigma) \propto \prod_i^N \prod_g^G \exp\left(-\frac{(y_i - f_g(\mathbf{x}_i))^2}{2\sigma^2}\right),$$

and with the prior specified in Section 3.1, we can formally write each prior as

$$p(\mathbf{\Gamma}) \propto \prod_g^G \prod_k^K p_g^{\gamma_{k,g}} (1 - p_g)^{1 - \gamma_{k,g}}$$

$$\begin{aligned}
p(\boldsymbol{\mu}) &\propto \prod_p^P \prod_k^K \exp\left(-\frac{\mu_{p,k}^2}{2\sigma_\mu^2}\right) \\
p(\boldsymbol{\theta}) &\propto \prod_k^K \exp\left(-\frac{\theta_k^2}{2\sigma_d^2}\right) \\
p(\alpha) &\propto \exp\left(-\frac{\alpha^2}{2\sigma_d^2}\right) \\
p(\sigma) &\propto \left(\hat{\sigma} \left[1 + \left(\frac{\sigma}{\hat{\sigma}}\right)^2\right]\right)^{-1}
\end{aligned}$$

The full proportional posterior is then given by:

$$\begin{aligned}
p(\boldsymbol{\Gamma}, \boldsymbol{\mu}, \boldsymbol{\theta}, \alpha, \sigma | \mathbf{y}) &\propto \prod_i^N \prod_g^G \prod_p^P \prod_k^K \left(\frac{1}{\sigma}\right) \exp\left(-\frac{(y_i - f_g(\mathbf{x}_i))^2 \sigma^2}{2\sigma^2}\right) \times p_g^{\gamma_{k,g}} (1 - p_g)^{1 - \gamma_{k,g}} \\
&\times \exp\left(-\frac{\mu_{p,k}^2}{2\sigma_\mu^2}\right) \times \exp\left(-\frac{\theta_k^2}{2\sigma_d^2}\right) \times \exp\left(-\frac{\alpha^2}{2\sigma_d^2}\right) \\
&\times \left(\hat{\sigma} \left[1 + \left(\frac{\sigma}{\hat{\sigma}}\right)^2\right]\right)^{-1}
\end{aligned}$$

In the next subsections, we discuss our posterior sampling algorithms, the specification of the prior hyperparameters, and other related computational details.

3.3 Posterior sampling

Our sampler iterates between the following steps:

1. **Updating α , $\boldsymbol{\theta}$:** The parameter α is updated by sampling from a normal distribution, $\alpha \sim \text{Normal}(\alpha_0 \sigma_0, \sqrt{\sigma_0})$. Here, α_0 is defined as $\sum_i (y_i - f_g(\mathbf{x}_i)) / \sigma^2$, and σ_0 as $(\sigma_d^{-2} + N / \sigma^2)^{-1}$. The full conditional of $\boldsymbol{\theta}$ is $\text{Normal}(\tilde{\boldsymbol{\theta}}, \mathbf{D})$, where $\tilde{\boldsymbol{\theta}} = \mathbf{D} (\sigma_d^{-2} \boldsymbol{\theta}_0 + \mathbf{X}^{*T} \mathbf{R} / \sigma^2)$ and $\mathbf{D} = (\sigma_d^{-2} \mathbf{I}_K + \mathbf{X}^{*T} \mathbf{X}^* / \sigma^2)^{-1}$. Here we define $\boldsymbol{\theta}_0 = (0, \dots, 0)^T$ and \mathbf{X}^* as a $N \times K$ matrix, where the i, k -th entry is $X_{i,k}^* = \gamma_{k,g} \exp\{-\frac{(\mathbf{x}_i - \boldsymbol{\mu}_k)^T (\mathbf{x}_i - \boldsymbol{\mu}_k)}{b_k^2}\}$, in which g is the corresponding treatment group for the i -th patient. We let the vector $\mathbf{R} = (R_1, \dots, R_n)$ be the residuals $R_i = y_i - \alpha$.

In cases of large values of K , the above-mentioned sampling method for $\boldsymbol{\theta}$ may not be efficient,

particularly when updating $\boldsymbol{\theta}$ from the full conditional where the k -th column of \mathbf{X}^* contains only 0. This condition implies that the corresponding k -th row of $\boldsymbol{\Gamma}$ is entirely 0. However, there is a strategic approach to mitigate this potential issue. When the k -th row of $\boldsymbol{\Gamma} = 0$, the full conditional of $\boldsymbol{\theta}$ simplifies to the prior distribution. We can then use a two-part sampling strategy for $\boldsymbol{\theta}$. We create a set of indices \mathcal{Z} such that the z -th row in which $\boldsymbol{\Gamma}$ contains only 0 for all $z \in \mathcal{Z}$, and sample θ_z from the prior distribution $\text{Normal}(0, \sigma_d^2)$. Let \mathcal{Z}^c be the complement set of indices. We sample $\boldsymbol{\theta}_{\mathcal{Z}^c}$ from the conditional $\text{Normal}(\tilde{\boldsymbol{\theta}}_{\mathcal{Z}^c}, \mathbf{D}_{\mathcal{Z}^c})$. In this case $\tilde{\boldsymbol{\theta}}_{\mathcal{Z}^c} = \mathbf{D}_{\mathcal{Z}^c} (\sigma_d^{-2} \boldsymbol{\theta}_{0, \mathcal{Z}^c} + \mathbf{X}_{\mathcal{Z}^c}^{*T} \mathbf{R} / \sigma^2)$, where $\mathbf{X}_{\mathcal{Z}^c}^{*T}$ is the submatrix from \mathbf{X}^* with columns from \mathcal{Z}^c , and $\mathbf{D}_{\mathcal{Z}^c} = (\sigma_d^{-2} \mathbf{I}_{|\mathcal{Z}^c|} + \mathbf{X}_{\mathcal{Z}^c}^{*T} \mathbf{X}_{\mathcal{Z}^c}^* / \sigma^2)^{-1}$, where $|\mathcal{Z}^c|$ denotes the number of entries \mathcal{Z}^c . This approach reduces computation time for large values of K .

2. **Updating $\boldsymbol{\Gamma}$:** Here, we consider full conditional Gibbs updates, where we update $\gamma_{k,g}$ in random order. We update $\gamma_{k,g}$ by sampling from a Bernoulli distribution, $\gamma_{k,g} \sim \text{Bernoulli}(\tilde{p}_g)$, where $\tilde{p}_g = \frac{p_g l_g^1}{p_g l_g^1 + (1-p_g) l_g^0}$. Here l_g^1 is the model likelihood when $\gamma_{k,g} = 1$ and likewise, l_g^0 is the model likelihood when $\gamma_{k,g} = 0$.
3. **Updating p_g :** We sample $p_g \sim \text{Beta}(c + \sum_g \gamma_{k,g}, d + K - \sum_g \gamma_{k,g})$. However, as discussed in Section 3.4, some of the indices are kept fixed for the first 1000 iterations of the MCMC and thus, the above posterior distribution is marginally adjusted by excluding those fixed indices.

We now describe the updates for $(\sigma$ and $\boldsymbol{\mu}_k)$, employing the Metropolis-Hastings (MH) sampling algorithm. For σ , we use the MH step as proposed in Linero and Yang (2018), while for $\boldsymbol{\mu}_k$ a gradient-based Langevin Monte Carlo (LMC) sampling algorithm is adopted. This approach is beneficial for complex hierarchical Bayesian model. We use superscript (t) to represent the corresponding posterior sample at the t -th iteration while describing the MH steps in detail below.

4. **Updating σ :** We implement the updating technique from Linero and Yang (2018). When imposing a flat prior for σ^{-2} , we can show that the conditional distribution for σ^{-2} is $\sigma^{-2} \sim \text{Ga}(1+N/2, \sum_g \sum_{i \in g} (R_i - f_g(\mathbf{x}_i))^2)$, where Ga stands for the gamma distribution. Under a flat prior, we can let this full conditional be our proposal distribution. This idea enables there to be a simplification in the acceptance probability, in which the acceptance probability conveniently becomes the ratio of priors. However, in order to integrate the proposal distribution in the

standard MH algorithm, we need to adjust the acceptance probability with the Jacobian transformation. Thus, we can accept the proposal with probability

$$A\left(\sigma^{(t)} \rightarrow \sigma'\right) = \frac{C^+(\sigma' | 0, \hat{\sigma}) \sigma'^3}{C^+(\sigma^{(t)} | 0, \hat{\sigma}) \sigma^{(t)3}} \wedge 1$$

5. **Updating μ_k :** To update μ_k , we use a gradient based sampler. The conditional posterior log-likelihood and its derivative with respect to $\mu_{p,k}$ are needed this process. The conditional posterior log-likelihood is given by

$$\log P(\mu_k | \mathbf{y}, \mathbf{\Gamma}, \boldsymbol{\theta}, \alpha, \sigma) = -\frac{n}{2} \log(2\pi\sigma^2) - \frac{1}{2\sigma^2} \sum_{i=1}^n (R_i - f_g(\mathbf{x}_i))^2 - \sum_{p=1}^P \frac{\mu_{p,k}^2}{2\sigma_\mu^2}.$$

The p -th entry of corresponding derivative $\nabla \log P(\mu_k | \mathbf{y}, \mathbf{\Gamma}, \boldsymbol{\theta}, \alpha, \sigma)$, with respect to $\mu_{p,k}$, is given by

$$\frac{2}{\sigma^2} \theta_k \gamma_{k,g} \sum_{i=1}^n \exp\left(-\sqrt{\frac{\sum_{p=1}^P (x_{i,p} - \mu_{p,k})^2}{b_k^2}}\right) \frac{\sum_{p=1}^P (x_{i,p} - \mu_{p,k})^2}{b_k^2} \left(\frac{x_{i,p} - \mu_{p,k}}{b_k^2}\right) - \frac{\mu_{p,k}}{\sigma_\mu^2}.$$

With gradient sampling, our proposed value now depends on the derivative, so that $\mu'_k = \mu_k^{(t)} + \frac{\epsilon}{2} \nabla \log P(\mu_k | \mathbf{y}, \mathbf{\Gamma}, \boldsymbol{\theta}, \alpha, \sigma) |_{\mu_k = \mu_k^{(t)}} + \delta$, where $\delta \sim \text{Normal}(0, \epsilon)$. Thus, the transition probability is

$$q(\mu'_k | \mu_k) \propto \exp\left(-\frac{1}{2\epsilon} \left\| \mu'_k - \mu_k - \frac{\epsilon}{2} \nabla \log P(\mu_k | \mathbf{y}, \mathbf{\Gamma}, \boldsymbol{\theta}, \alpha, \sigma) \right\|_2^2\right),$$

and then the acceptance probability for our gradient sampler for a proposed value μ' is

$$A\left(\mu_k^{(t)} \rightarrow \mu'_k\right) = \frac{P(\mu'_k | \mathbf{y}, \mathbf{\Gamma}, \boldsymbol{\theta}, \alpha, \sigma) q(\mu_k^{(t)} | \mu'_k)}{P(\mu_k^{(t)} | \mathbf{y}, \mathbf{\Gamma}, \boldsymbol{\theta}, \alpha, \sigma) q(\mu'_k | \mu_k^{(t)})} \wedge 1.$$

The proposal values for $\mu_{p,k}$ are adjusted to achieve a pre-specified acceptance rate, tuning ϵ every 200 iterations to maintain an acceptance rate between 0.45 and 0.7.

3.4 Specification of K

Our approach here relies on the empirical Bayes-type scheme, discussed in Roy (2023). We first create an index list to group the response and predictors associated with the g -th treatment. For each treatment group, we utilize Gaussian RBF kernel-based relevance vector machine (RVM) within the `rvm` function within the R package `kernlab` (Karatzoglou et al., 2004), which provides the group-specific number of relevance vectors v_g . We then set $K = G \times \max_g v_g$, combining all the outputs of `rvm`.

Our initialization of $\mathbf{\Gamma}$ depends on both v_g and K . While executing this step, we first specify G disjoint sets, denoted as $\{\mathcal{I}_1, \dots, \mathcal{I}_G\}$. We have $\mathcal{I}_g \cap \mathcal{I}_{g'} = \emptyset$ for all $g \neq g'$ and $\cup_{g=1}^G \mathcal{I}_g \subset \{1, 2, \dots, K\}$. These are a small set of indices such that $\gamma_{k,g}$ is fixed at 1 for all $k \in \mathcal{I}_g$ at the initial stage of the MCMC. The set \mathcal{I}_g is constructed as $\mathcal{I}_g = \{k + \sum_{t=1}^{g-1} v_t : k \in \{1, 2, \dots, v_g\}\}$. For the first 1000 iterations, we only sample $\gamma_{k,g}$ for $k \notin \mathcal{I}_g$, and then for all k afterwards.

The initialization of the RBF centers $\boldsymbol{\mu}$ relies on the entropy-weighted k-means (EWKM) clustering algorithm. The EWKM algorithm is based on traditional k-means clustering by incorporating an entropy-based weighting scheme (Jing et al., 2007). We implement the algorithm through the `ewkm` function from the `wskm` package in R (Williams et al., 2020), where we set K as the target number of centers. The function returns the centroids of the clusters, computed as the weighted mean position of all points in each cluster. We then add a small amount of random noise (from the normal distribution) to the centroids for stability, as some of the centers turn out to be identical in the `ewkm` output. The final adjusted centroids serve as our initialization for $\boldsymbol{\mu}_k$'s and thus, $\boldsymbol{\mu}$. We now discuss the associated computational steps and our scheme of inference.

3.5 Other computational settings

Our calibration of the prior hyperparameters follows some of the data-driven strategies proposed in Chipman et al. (2010) and Linero and Yang (2018). We first apply min-max transformation on the response as, $(\mathbf{y} - \min(\mathbf{y}) - 0.5(\max(\mathbf{y}) - \min(\mathbf{y}))) / (\max(\mathbf{y}) - \min(\mathbf{y}))$ which makes it bounded in $[-0.5, 0.5]$. After fitting the model, we apply an inverse transformation on the estimated f_g 's. For the covariates \mathbf{x} , we use a similar transformation $(\mathbf{x} - \min(\mathbf{x})) / (\max(\mathbf{x}) - \min(\mathbf{x}))$ to bound them within $[0, 1]$. Under the RBF-net model, the expectation of a response given the covariate

\mathbf{x} with K_1 bases is $\sum_{k=1}^{K_1} \theta_k \exp\{-(\mathbf{x} - \boldsymbol{\mu}_k)^T(\mathbf{x} - \boldsymbol{\mu}_k)/b_k^2\}$. For a random variable distributed as $\text{Normal}(\mu, \sigma^2)$, most of its mass falls within $\mu \pm 1.96\sigma$. Furthermore, the maximum value of $\exp\{-(\mathbf{x}_i - \boldsymbol{\mu}_k)^T(\mathbf{x}_i - \boldsymbol{\mu}_k)/b_k^2\}$ is 1. Thus, the value of $\sum_{k=1}^{K_1} \theta_k \exp\{-(\mathbf{x} - \boldsymbol{\mu}_k)^T(\mathbf{x} - \boldsymbol{\mu}_k)/b_k^2\}$ will be within $0 \pm 1.96\sigma_d\sqrt{K_1}$ if $\theta_k \sim \text{Normal}(0, \sigma_d^2)$. Our min-max normalized data satisfies $|y_{\min}| = |y_{\max}| = 0.5$. Thus, we may set $0.5 = 1.96\sigma_d\sqrt{K_1}$. Hence approximately, $\sigma_d = 1/(4\sqrt{K_1}) = 1/(\sqrt{16K_1})$.

Now, in our case, the numbers of active bases are different for different $f_g(\cdot)$'s. For group g , we have $\sum_{k=1}^K \gamma_{k,g}$ bases. We, thus, consider to initialize K_1 as $K_1 = \max_g \sum_{k=1}^K \gamma_{k,g}$, based on our initialization of $\boldsymbol{\Gamma}$. In the above expression ($\max_g \sum_{k=1}^K \gamma_{k,g}$) for setting K_1 , one may consider mean or median over g too, as we do not necessarily need K_1 to be an integer here. However, this value may not remain appropriate once other parameters start updating. Thus, we re-calculate the above expression of K_1 in the middle of the burn-in phase of our MCMC chain. Afterwards, we set K_1 as K for every 200 iterations.

For the initialization of some of our parameters, $\boldsymbol{\theta}$ is set as the least squares estimate. For probability p_g , we initially set $p_g = 1/2$ for all g to allow an equal likelihood for all $k \in \mathcal{I}_g$, as described in Section 3.4, to be included. The bandwidth parameters b_k 's are also pre-specified. For simplicity, we let $b_k = b$ for all k . Then, we first initialize $\boldsymbol{\mu}$ as discussed in Section 3.4 and set: $b = \frac{\sqrt{2}}{k(k-1)} \sum_{i=1}^{k-1} \sum_{j=i+1}^k \|\boldsymbol{\mu}_i - \boldsymbol{\mu}_j\|_2$, where $\|\cdot\|_2$ represents the Euclidean norm and $\boldsymbol{\mu}_j$ is j -th column of $\boldsymbol{\mu}$. Some of the prior hyperparameters are set as $\sigma_\mu = 1, c = d = 1$.

3.6 Inference for CATE using linear projections and thresholding

Following Semenova and Chernozhukov (2021); Cui et al. (2023), we adopt a linear projection-based approach for the inference on $\tau(\cdot)$ to circumvent the difficulties in non-parametric inferences. Projections can provide a meaningful interpretation and summary of treatment heterogeneity, as argued in Semenova and Chernozhukov (2021). The best linear projection (BLP) of $\tau(\cdot)$ given a set of covariates \mathbf{x}_i is defined as

$$\{\beta_0^*, \boldsymbol{\beta}^*\} = \operatorname{argmin}_{\beta_0, \boldsymbol{\beta}} \mathbb{E} \left[(\tau(\mathbf{x}_i) - \beta_0 - \mathbf{x}_i \boldsymbol{\beta})^2 \right],$$

where β_0^* and β^* are the intercept and the coefficient estimates our covariates, respectively. One can estimate the BLP parameters by regressing the CATE estimates $\hat{\tau}(\mathbf{x}_i)$ on \mathbf{x}_i .

We modify this approach a bit for our Bayesian setting. When there are three treatments as in our numerical experiment and MIMIC data application, we may be interested in τ_{21} and τ_{31} , quantifying the effects of treatment-2 over treatment-1 and 3 over 1, respectively. Then, for the s -th posterior sample, we obtain $\hat{\tau}_{21,s}(\mathbf{x}_i)$ and $\hat{\tau}_{31,s}(\mathbf{x}_i)$, based on the posterior samples of f_g 's for the i -th patient. We then separately regress $\hat{\tau}_{21,s}(\mathbf{x})$ and $\hat{\tau}_{31,s}(\mathbf{x})$ on \mathbf{x} , providing the estimated BLP coefficients for each predictor corresponding to s -th posterior sample. Collecting all the obtained BLP coefficients across posterior samples, we calculate the equal-tail 95% credible interval for each predictor. Predictors for which the credible interval excludes 0 are considered important.

In addition, we extend the above approach by first thresholding the regression coefficients and then computing the credible intervals. This will enable us to order the predictors based on their importance. Specifically, for our MIMIC data analysis, we generate B resampled datasets with the same number of data points as in the original data by sampling with replacement similar to bootstrap and then compute the thresholding-based credible intervals $\mathcal{C}_{p,b,t}$'s for each predictor p , dataset b and threshold t . Finally, for a given predictor p and threshold t , we compute $s_{p,t} = \frac{1}{B} \sum_{b=1}^B \mathbf{1}\{0 \notin \mathcal{C}_{p,b,t}\}$, the proportion of credible intervals not containing 0 across all the datasets. It is easy to see that as t increases, $s_{p,t}$ will decrease, providing us a measure of importance for each predictor. A larger value of $s_{p,t}$ would indicate the higher importance of p -th predictor under the level of threshold at t . In simulation case 4.2, we evaluate this procedure based on B independently replicated datasets.

4 Simulation

In this section, we assess the effectiveness of our proposed RBF method by estimating model parameters using the training data and calculating predicted mean square errors on the test set. We compare these results with other methods. The mean square error (MSE) is defined as $\frac{1}{s} \sum_{r=1}^s \frac{1}{|T_r|} \sum_{i \in T_r} (\tau_r - \hat{\tau}_r)^2$, where T_r represents the test set for the r -th replication.

We conduct two simulations with 30 replicated datasets, dividing each dataset into testing and training sets with a ratio of 67/33. In the first simulation, we consider two sample sizes 180 and

360 with 5 predictors ($P = 5$) whose entries are generated from $\text{Unif}(0, 1)$. The second simulation employs predictors and treatments sourced from the MIMIC-III database.

For our method, we generate 10000 MCMC samples after burning in the first 5000. We then perform thinning by selecting every 10-*th* sample, resulting in 1000 posterior samples. For our predictive comparison, we first obtain the predictions for each posterior sample and take the average over all the samples.

In each case, we compare our estimates with a multi-arm causal forest from the `grf` (Tibshirani et al., 2023) package-based solution. Training and testing a causal forest with the the `grf` package requires `multi_arm_causal_forest` and `predict.multi_arm_causal_forest` function on the training and testing set, respectively. The CATE estimation can then be extracted from the predictions (Tibshirani et al., 2023). To the best of our knowledge, there is no other package that supports CATE estimation for more than two treatments for out-of-sample predictors. Alternatively, we fit treatment-specific separate functions and get the treatment-effect estimates by taking their differences, as done in T-learning. Our candidate models for this approach are relevance vector machine (RVM), support vector regression (SVR), ordinary least square (OLS), and BART. For the competing methods, we use the R packages that include `e1071R` (Meyer et al., 2019), `BART`(McCulloch et al., 2019), `kernlab` (Karatzoglou et al., 2004), and few other functions from the base packages of R.

The outcome \mathbf{y} is generated by y_i from $\text{Normal}(f_g(\mathbf{x}_i), 1)$, where three treatment-outcome functions $f_1(\cdot), f_2(\cdot), f_3(\cdot)$ are

$$\begin{aligned} f_1(\mathbf{x}) &= f_1^0(\mathbf{x}) + f_2^0(\mathbf{x}) \\ f_2(\mathbf{x}) &= (f_1^0(\mathbf{x}) + f_2^0(\mathbf{x}))/2 + f_3^0(\mathbf{x})/3 \\ f_3(\mathbf{x}) &= (f_2^0(\mathbf{x}) + f_3^0(\mathbf{x}))/2 + f_1^0(\mathbf{x})/3 \end{aligned}$$

These functions have commonalities based on the individual regression functions:

$$\begin{aligned} f_1^0(\mathbf{x}) &= 10 \sin(\pi x_1 x_2) + 20(x_3 - 0.5)^2 + (10x_4 + 5x_5) \\ f_2^0(\mathbf{x}) &= (5x_2)/(1 + x_1^2) + 5 \sin(x_3 x_4) + x_5 \\ f_3^0(\mathbf{x}) &= 0.1 \exp(4x_1) + 4/(1 + \exp(-20(x_2 - 0.5))) + 3x_3^2 + 2x_4 + x_5 \end{aligned}$$

4.1 Setting 1

In our evaluation, we consider two scenarios, each characterized by sample sizes 180 and 360. For each scenario, we create three equal treatment groups and generate 30 replicated datasets. To assess the performance of our model, each dataset is partitioned into training and testing sets with a 67/33 split.

The results, as detailed in Table 1, demonstrate the efficacy of our proposed method. Notably, our approach consistently outperforms T-learning-type models, where treatment-specific separate outcome functions are fitted. This is particularly evident in the scenario with the smaller sample size. When comparing our method to the multi-arm causal forest, we observe that while our method exhibits superior performance in the small sample size case, the results are relatively comparable for the larger sample size scenario. This suggests that our model’s advantages are more pronounced in situations with limited data, a crucial aspect for practical applications where large datasets may not be readily available.

Table 1: Comparing estimation errors for the two treatment contrasts τ_{21} and τ_{31} across different methods, based on 30 replications and two choices for the total sample size under Simulation setting 1. The errors for the T-learning type models are separated from the two multi-treatment cases with a horizontal line. The reported errors are the medians over all replications.

	$n = 180$		$n = 360$	
	$\hat{\tau}_{21}$ MSE	$\hat{\tau}_{31}$ MSE	$\hat{\tau}_{21}$ MSE	$\hat{\tau}_{31}$ MSE
Shared-neuron RBF	2.88	5.03	3.42	4.46
Causal Random Forest	5.33	10.08	2.51	5.43
RVM	14.73	11.11	8.55	9.90
SVR	5.58	7.03	8.98	8.87
OLS	8.80	9.01	4.91	5.86
BART20	14.49	8.78	10.34	9.15
BART50	14.67	7.84	9.86	8.57
BART200	15.19	7.75	10.60	8.28

4.2 Setting 2

In Setting 1, the assignment of the treatment groups and the generation of the predictors are performed independently. We now transition to using the predictors and treatment assignments from the MIMIC-III database, enabling us to evaluate our model in the presence of unknown,

complex dependencies among the predictors and treatment assignments that are anticipated in the MIMIC data. From the MIMIC dataset, we constructed three treatment groups based on the usage of only mechanical ventilation (group 1), only vasopressor (group 2), and both (group 3). Further details are provided in Section 5. Our final dataset in our real data analysis comprises of 172 subjects and 15 predictors. However, for this simulation experiment, we pick a subset of predictors out of these 15, employing the marginal screening approach from Xue and Liang (2017) based on the two outcomes: the length of stay in the Intensive Care Unit (LOS-ICU) and Sequential Organ Failure Assessment (SOFA) scores. We pick the top five most important predictors for each outcome, and after taking the union, we find the following set of key predictors: age, weight, bicarbonate level, sodium level, systolic blood pressure (SBP), potassium level, and mean arterial pressure (MAP).

We then generate \mathbf{y} in the same manner as in the preceding section based on the first five predictors age, weight, bicarbonate level, sodium level, and SBP, excluding potassium level and mean arterial pressure (MAP). However, while fitting the model, we include all seven predictors and evaluate their importance subsequently. We would like to mention here that the selection of predictors for this simulation does not necessarily need the marginal screening procedure. It is done to conduct this selection step systematically and include the most important predictors associated with our primary outcomes in Section 5.

The true outcome functions are identical to those in Section 4.1. Table 2 presents an MSE comparison of the CATE estimates of our method versus other competing methods. As in the sample size case of Section 4.1, our model again performs better than the multi-arm casual forest approach. Among the T-learning-type methods, our proposed method excels in all but the support vector regression method.

Furthermore, we apply the projection-based inference method from Section 3.6. Specifically, our \mathbf{y} , here, only depends on the first five predictors listed earlier, and not on potassium and MAP. Table 3 displays the average BLP coefficient for each predictor under both of two treatment contrasts across all the replications. We also report the proportion of replicated datasets that correspond to credible intervals containing zero. Here, we find that six out of seven predictors were deemed significant in all 30 replications. Only one predictor, potassium, is found insignificant across almost all replications.

We now turn to our thresholding-based credible interval comparison approach from Section 3.6 based on the $s_{p,t}$ -values for different predictors (p) and threshold (t). Four choices for the thresholding value (t) are considered 0.5, 0.8, 1, and 2. Table 4 shows the $s_{t,p}$ -values based on 30 replications for τ_{23} and τ_{13} , respectively. As expected, the decrease in $s_{p,t}$ with t is the sharpest for potassium and MAP, which aligns with their exclusion from the data generation process. The $s_{p,t}$ -values thus provide useful insights into the relationship between the outcome and the predictors.

Table 2: Comparing estimation errors for the two treatment contrasts τ_{23} and τ_{13} across different methods, based on 30 replications and two choices for the total sample size under Simulation setting 2. The errors for the T-learning type models are separated from the two multi-treatment cases with a horizontal line. The reported errors are the medians over all replications.

	$\hat{\tau}_{23}$ MSE	$\hat{\tau}_{13}$ MSE
Shared-neuron RBF	3.09	4.95
Causal Random Forest	4.66	10.70
RVM	11.92	9.74
SVR	2.74	4.46
OLS	8.04	10.55
BART20	10.89	11.85
BART50	10.41	11.59
BART200	9.73	11.50

Table 3: The average posterior mean of the Best Linear Projection Coefficients are reported, along with their average exclusion proportion of zeros within the credible interval ($s_{p,0}$ -values).

Predictor	$\hat{\tau}_{23}$	$\hat{\tau}_{13}$
Intercept	10.96 (1.00)	11.90 (1.00)
Age	-10.96 (1.00)	-11.29 (1.00)
Weight	-3.90 (1.00)	-4.00 (1.00)
Bicarbonate)	-9.23 (1.00)	-9.22 (1.00)
Sodium	-3.94 (1.00)	-3.75 (1.00)
Systolic Blood Pressure	-3.81 (1.00)	-4.14 (1.00)
Potassium	-1.03 (0.10)	-1.01 (0.13)
Mean Arterial Pressure	-2.25 (1.00)	-2.10 (1.00)

Table 4: Comparison of thresholding-based $s_{p,t}$ -values for $\hat{\tau}_{23}$ and $\hat{\tau}_{13}$ for different choices of thresholds (t), and predictors. The thresholding levels are given in the first column. The generated outcomes are independent of the last two predictors. The exclusion proportions are based on 30 replicated datasets.

$\hat{\tau}_{23}$	Intercept	SBP	Bicarbonate	Sodium	Age	Weight	Potassium	MAP
Threshold = 0.5	1.00	0.93	1.00	0.87	1.00	1.00	0.03	0.97
Threshold = 0.8	1.00	0.90	1.00	0.87	1.00	1.00	0.00	0.80
Threshold = 1.0	1.00	0.90	1.00	0.83	1.00	1.00	0.00	0.73
Threshold = 1.5	1.00	0.57	1.00	0.57	1.00	0.97	0.00	0.37
Threshold = 2.0	1.00	0.23	1.00	0.17	1.00	0.73	0.00	0.13
$\hat{\tau}_{13}$								
Threshold = 0.5	1.00	0.97	1.00	0.93	1.00	1.00	0.03	0.93
Threshold = 0.8	1.00	0.90	1.00	0.87	1.00	1.00	0.00	0.77
Threshold = 1.0	1.00	0.90	1.00	0.83	1.00	1.00	0.00	0.67
Threshold = 1.5	1.00	0.83	1.00	0.53	1.00	0.97	0.00	0.33
Threshold = 2.0	1.00	0.47	1.00	0.20	1.00	0.77	0.00	0.13

5 MIMIC Data Analysis

MIMIC-III is a large single-center database, containing deidentified, comprehensive clinical data of patients admitted to the Beth Israel Deaconess Medical Center in Boston, Massachusetts (Johnson et al., 2016). With 53,423 distinct hospital admissions for adults in critical care units from 2001 to 2012, the dataset offers a vast amount of patient information, encompassing demographics, laboratory results, medicine summaries, and diagnostic codes. This extensive data allows us to employ our RBF-net with shared neurons for septic patients. With the most current revision, sepsis is defined following Singer et al. (2016) as a *life-threatening* condition resulting from dysregulated host responses to infection, often identified by a Sequential [Sepsis-related] Organ Failure Assessment (SOFA) score increase of 2 points or more. The progression of sepsis can lead to septic shock, characterized by profound circulatory, cellular, and metabolic abnormalities.

In our analysis, we focus on septic patients, specifically gathering information from the first 12 hours of their initial visit while excluding any subsequent readmissions. The criteria for identifying sepsis encompass patients diagnosed with “Sepsis”, “Septic shock”, or “Severe sepsis” during their inaugural visit. We further refine our cohort to include only those who were discharged to their “home”. One challenge regarding MIMIC-III, and electronic health records in general is the amount of missing data (Groenwold, 2020). To handle missing data in MIMIC-III (Hou et al., 2020; Li et al., 2021), we screen variables and remove those with over 20% missing. We also use a

hybrid procedure by applying the last observation carried forward (LOCF) first and then multiple imputations to handle this issue (Jazayeri et al., 2020). The chosen predictors for our analysis include age, weight, hemoglobin, white blood cells, blood urea nitrogen (BUN), potassium, sodium, bicarbonate, creatinine, platelet count, heart rate, systolic blood pressure (SBP), diastolic blood pressure (DBP), mean arterial pressure (MAP), and temperature. Among these variables, the maximum percentage of missing is found to be 8.14% for the ‘white blood cell’ variable as shown in Table 5. As discussed in Section 4.2, our treatment groups are based on the usage of only mechanical ventilation (group 1), only vasopressor (group 2), and both (group 3). Tables 5 and 6 are the demographics for our study population, with Table 6 stratifying by treatment group. The demographics contain the mean and standard deviation of both the predictors and outcomes.

For each predictor with missing observations, LOCF is applied using `na.locf` function from the R package `zoo` (Zeileis and Grothendieck, 2005) for each patient. However, some patients do not have observations in the initial hours of their visit. Thus, LOCF is not adequate to impute all the missing values. For the rest of the missing values, we consider multiple imputations using the R package `mice` (van Buuren and Groothuis-Oudshoorn, 2011). Similar to our approach in Section 4, we generate 1000 posterior samples from an original pool of 15000 samples, incorporating a burn-in phase of 5000 samples and a thinning by taking every 10-*th* samples.

For our analysis, we consider two possible outcomes, the length of ICU stay and the 12-*th* hour SOFA score. We initially fit the model for both of the two outcomes in their original scale and the log scale. However, after examining the distributions of the residuals, we only consider reporting our results for the LOS-ICU in log scale and SOFA scores with a square root transformation as their residuals uphold the normality assumption. To further confirm the normality of the residuals, we perform the Shapiro-Wilks test using `shapiro.test` in R. The residual density plots are provided in Figures 1 and 2 in the supplementary material. Given the challenges in comparing predictive performance with real data, our analysis primarily centers on covariate inferences. For each choice of outcome, we obtain the BLP estimate for each covariate with their credible interval to identify the important predictors for both $\hat{\tau}_{23}$ and $\hat{\tau}_{13}$. Table 7 displays the credible intervals for the outcomes. Notably, MAP and SBP are identified as significant predictors for $\hat{\tau}_{23}$ for LOS-ICU and SOFA scores, respectively. Similarly, for $\hat{\tau}_{13}$, SBP remains significant when SOFA scores are the outcome. However, no significant predictors are observed for $\hat{\tau}_{13}$ when LOS-ICU is the outcome.

Table 5: Overall Demographics for Selected Septic Patients in MIMIC-III Database. Predictor variables reported represent the average value after 12 hours of observation in hospital. Outcome variables reported represent the value at the 12th hour. We also report the amount of missing values in each group before applying LOCF and imputation to complete the data.

Variable	Overall	
	Mean (SD)	% Missing
Age	53.8 (17.78)	0%
Bicarbonate	20.04 (4.15)	4.65%
BUN	25.43 (18.68)	4.65%
Creatinine	1.58 (1.54)	4.65%
DBP	60.57 (8.67)	0%
Hemoglobin	10.86 (1.81)	7.56%
Heart Rate	93.26 (17.91)	0%
Potassium	4.04 (0.67)	4.65%
Platelet Count	191.86 (104.14)	7.56%
MAP	73.74 (9.15)	0%
SBP	107.58 (11.97)	0%
Sodium	138.86 (3.6)	5.23%
Temperature	37.06 (0.82)	0%
Weight	82.29 (21.67)	2.91%
White Blood Cell	14.9 (8.44)	8.14%
Length of Stay in ICU	4.47 (4.01)	0%
SOFA Score	6.96 (2.82)	0%

Tables 1 and 2 in the supplementary materials summarize similar results for comparing the other possible treatment pairs.

The exclusion proportions of each covariate using 50 resampled datasets on applying the thresholding approach are presented in Table 8. In examining these proportions for thresholding-based $s_{p,t}$ -values for $\hat{\tau}_{23}$ and $\hat{\tau}_{13}$ with respect to LOS-ICU on log scale and square-root transformed SOFA score, a pattern aligns with the results of credible intervals. Both MAP and SBP display the highest amount of exclusion proportions among all predictors, establishing the significance of these two variables despite resampling. For instance, in the context of $\hat{\tau}_{23}$ for LOS-ICU and SOFA scores, MAP is a significant predictor 68% and 48% of the time, while SBP is found to be significant in 50% and 74% of those datasets for $\hat{\tau}_{23}$ with LOS-ICU and SOFA scores. In the context of $\hat{\tau}_{13}$, the respective exclusion proportions for predictors MAP and SBP are 0.46 and 0.80 for SOFA scores.

Furthermore, Table 8 complements Table 7 by ordering the significance of predictors for MAP

Table 6: Treatment group-specific summaries of the covariates for selected sets of septic patients in the MIMIC-III database are illustrated here. For all the predictor variables, the reported statistics are based on the first 12-hour averages under ICU. The statistics on the SOFA score are evaluated based on the value at the 12th hour in the ICU.

	Ventilator Only	Vasopressor Only	Both
Variable	Mean (SD)	Mean (SD)	Mean (SD)
Age	53.88 (19.41)	46.7 (16.18)	57.49 (16.63)
Bicarbonate	18.96 (4.79)	21.48 (4.91)	19.85 (3.02)
BUN	28.96 (21.08)	23.84 (22.50)	24.13 (14.44)
Creatinine	1.68 (1.06)	1.42 (1.56)	1.62 (1.76)
DBP	59.78 (8.87)	64.56 (9.72)	59.01 (7.48)
Hemoglobin	11.4 (2.28)	10.82 (1.73)	10.58 (1.50)
Heart Rate	93.96 (18.48)	99.72 (18.78)	89.57 (16.27)
Potassium	4.23 (0.78)	4.07 (0.62)	3.88 (0.60)
MAP	73.27 (9.07)	79.62 (11.58)	71.07 (5.84)
Sodium	138.71 (4.02)	139.21 (4.34)	138.84 (3)
Platelet Count	191.44 (89.81)	212.27 (128.32)	181.59 (98.06)
SBP	105.43 (8.76)	117.01 (16.85)	104.17 (6.96)
Temperature	37.02 (0.82)	37.19 (0.76)	37.0 (0.76)
White Blood Cell	13.36 (7.41)	15.06 (9.12)	15.65 (8.72)
Weight	84.99 (26.85)	86.15 (25.24)	78.95 (15.51)
Length of Stay in ICU	6.14 (3.91)	6.43 (5.5)	2.48 (1.39)
SOFA Score	8.98 (2.82)	6.05 (2.8)	6.28 (2.22)

and SBP. For LOS-ICU, there is a higher proportion of exclusions for MAP than SBP, indicating a greater significance for that particular outcome. Conversely, for SOFA scores, SBP is excluded more than MAP, making it more significant than MAP. This thorough analysis illustrates not only the significance but also the relative importance of predictors for LOS-ICU and SOFA scores.

6 Discussion

In this article, we addressed the challenge of estimating heterogeneous treatment effects in scenarios with more than two treatment groups, particularly when treatment responses exhibit shared characteristics. By tackling this problem, we can create efficient individualized treatments. We developed a radial basis functions-based model to integrate both similarities and variations in treatment outcomes. Our proposed model approaches this through the parameter Γ , which crucially controls the bases to be used in specifying an outcome under a given treatment. We obtain outstanding numerical results, demonstrating the superior performance of our method compared to various other

Table 7: The 95% credible intervals of the BLP coefficients for predictors in MIMIC-III for $\tau_{23}(\mathbf{x})$ and $\tau_{13}(\mathbf{x})$ for log-transformed length of stay in the ICU and square-root transformed 12-th hour SOFA score. Treatment groups are based on the usage of only mechanical ventilation (group 1), only vasopressor (group 2), and both (group 3).

Variable	$\hat{\tau}_{23}$		$\hat{\tau}_{13}$	
	log(LOS-ICU)	$\sqrt{\text{SOFA Score}}$	log(LOS-ICU)	$\sqrt{\text{SOFA Score}}$
Intercept	(-2.524, 1.055)	(-0.831, 0.188)	(-0.444, 0.388)	(-0.912, 0.187)
Age	(-0.184, 0.314)	(-0.098, 0.037)	(-0.083, 0.102)	(-0.107, 0.033)
Bicarbonate	(-0.244, 0.174)	(-0.200, 0.051)	(-0.061, 0.076)	(-0.185, 0.167)
BUN	(-0.182, 0.212)	(-0.111, 0.130)	(-0.058, 0.049)	(-0.242, 0.111)
Creatinine	(-0.398, 0.112)	(-0.175, 0.176)	(-0.083, 0.046)	(-0.389, 0.142)
DBP	(-0.317, 0.201)	(-0.078, 0.070)	(-0.104, 0.087)	(-0.125, 0.063)
Hemoglobin	(-0.141, 0.345)	(-0.127, 0.023)	(-0.094, 0.115)	(-0.125, 0.054)
Heart Rate	(-0.538, 0.119)	(-0.103, 0.032)	(-0.235, 0.159)	(-0.118, 0.030)
MAP	(-0.413, -0.025)	(-0.116, 0.014)	(-0.095, 0.076)	(-0.161, 0.002)
Potassium	(-0.203, 0.245)	(-0.077, 0.108)	(-0.051, 0.061)	(-0.154, 0.095)
Platelet Count	(-0.169, 0.295)	(-0.247, 0.168)	(-0.054, 0.066)	(-0.214, 0.422)
SBP	(-0.066, 0.452)	(0.031, 0.187)	(-0.075, 0.104)	(0.042, 0.220)
Sodium	(-0.299, 0.130)	(-0.065, 0.055)	(-0.059, 0.065)	(-0.066, 0.064)
Temperature	(-0.222, 0.199)	(-0.086, 0.053)	(-0.047, 0.040)	(-0.086, 0.074)
Weight	(-0.249, 0.225)	(-0.030, 0.125)	(-0.061, 0.056)	(-0.073, 0.118)
White Blood Cell	(-0.119, 0.310)	(-0.059, 0.060)	(-0.064, 0.060)	(-0.054, 0.060)

competing methods for CATE estimation.

The findings in the MIMIC data analysis emphasize the critical role of mean arterial pressure and systolic blood pressure as predictors, consistently identified as significant across different analytical methods and outcomes in our study. The results from the credible intervals reveal that mean arterial pressure and systolic blood pressure are significant for outcomes LOS-ICU and SOFA scores using the best linear projection method. For the length of stay in the ICU, the negative credible interval associated with MAP indicates a higher MAP is linked with a lower duration in the ICU. Similarly, the positive credible interval linked to SBP suggests a higher SBP correlates to higher SOFA scores. Furthermore, our thresholding-based approach show that MAP and SBP have the highest exclusion proportion of 0 within the credible intervals among all other predictors, highlighting the importance of these two variables. Some of the past studies have found them significantly associated with ICU mortality and SOFA scores (Kenzaka et al., 2012; Sarkar et al., 2022; Khanna et al., 2023).

The results specifically guide us toward identifying appropriate treatment strategies. For patients with a higher MAP values, a treatment of administering a vasopressor is preferable than

Table 8: Comparison of exclusion proportions for thresholding-based $s_{p,t}$ -values for $\hat{\tau}_{23}$ and $\hat{\tau}_{13}$ for log(LOS-ICU) and SOFA Score for different choices of thresholds (t), and predictors using 50 resampled datasets. The thresholding levels are given in the first row. Treatment groups are based on the usage of only mechanical ventilation (group 1), only vasopressor (group 2), and both (group 3).

Variable	$\hat{\tau}_{23}$				$\hat{\tau}_{13}$			
	log(LOS-ICU)		$\sqrt{\text{SOFA Score}}$		log(LOS-ICU)		$\sqrt{\text{SOFA Score}}$	
	Threshold							
	0	0.5	0	0.5	0	0.5	0	0.5
Intercept	0.02	0.00	0.08	0.00	0.00	0.00	0.10	0.00
Age	0.08	0.00	0.22	0.00	0.02	0.00	0.22	0.00
Bicarbonate	0.22	0.00	0.08	0.00	0.00	0.00	0.12	0.00
BUN	0.20	0.00	0.06	0.00	0.00	0.00	0.12	0.00
Creatinine	0.12	0.00	0.02	0.00	0.00	0.00	0.08	0.00
DBP	0.26	0.00	0.22	0.00	0.00	0.00	0.16	0.00
Hemoglobin	0.18	0.00	0.18	0.00	0.00	0.00	0.08	0.00
Heart Rate	0.26	0.00	0.10	0.00	0.00	0.00	0.12	0.00
MAP	0.68	0.00	0.48	0.00	0.00	0.00	0.46	0.00
Potassium	0.08	0.00	0.00	0.00	0.00	0.00	0.02	0.00
Platelet Count	0.12	0.00	0.04	0.00	0.00	0.00	0.08	0.00
SBP	0.50	0.00	0.74	0.00	0.00	0.00	0.80	0.00
Sodium	0.28	0.02	0.00	0.00	0.02	0.00	0.02	0.00
Temperature	0.10	0.00	0.04	0.00	0.00	0.00	0.04	0.00
Weight	0.14	0.00	0.16	0.00	0.00	0.00	0.12	0.00
White Blood Cell	0.20	0.00	0.22	0.00	0.02	0.00	0.18	0.00

using both mechanical ventilation and a vasopressor, potentially leading to a shorter length of stay in the ICU. At the same time, utilizing both mechanical ventilation and a vasopressor is preferable than employing either just mechanical ventilation or a vasopressor for patients with higher SBP values. Thus, our study suggest that they are important predictors for determining an optimal treatment plan among these three treatment groups.

Looking ahead, we hope to potentially broaden our model’s application. The shared basis construction can be generalized to other types of models as well. Like in tree-based models, one may allow sharing of trees. Another direction will be to extend the proposed architecture to model other types of outcomes, such as right-censored survival data or binary or count-valued data. Another possible extension of the proposed model is to incorporate the covariate effect into p_g . These future directions help to further the scope and impact of our work in the field of personalized medicine. Codes to fit the model with examples from Section 4 are in <https://github.com/pshuwei/RBF>.

References

- Brown, D. W., DeSantis, S. M., Greene, T. J., Maroufy, V., Yaseen, A., Wu, H., Williams, G., and Swartz, M. D. (2020), “A novel approach for propensity score matching and stratification for multiple treatments: Application to an electronic health record–derived study,” *Statistics in medicine*, 39(17), 2308–2323.
- Chalkou, K., Steyerberg, E., Egger, M., Manca, A., Pellegrini, F., and Salanti, G. (2021), “A two-stage prediction model for heterogeneous effects of treatments,” *Statistics in medicine*, 40(20), 4362–4375.
- Cheng, D., Chakraborty, A., Ananthakrishnan, A. N., and Cai, T. (2020), “Estimating average treatment effects with a double-index propensity score,” *Biometrics*, 76(3), 767–777.
- Chernozhukov, V., Chetverikov, D., Demirer, M., Dufo, E., Hansen, C., Newey, W., and Robins, J. (2018), “Double/debiased machine learning for treatment and structural parameters,” *The Econometrics Journal*, 21(1), C1–C68.
- Chipman, H. A., George, E. I., and McCulloch, R. E. (2010), “BART: Bayesian additive regression trees,” *The Annals of Applied Statistics*, 4(1), 266–298.
- Cui, Y., Kosorok, M. R., Sverdrup, E., Wager, S., and Zhu, R. (2023), “Estimating heterogeneous treatment effects with right-censored data via causal survival forests,” *Journal of the Royal Statistical Society Series B: Statistical Methodology*, 85(2), 179–211.
- Cui, Y., and Tchetgen Tchetgen, E. (2021), “A semiparametric instrumental variable approach to optimal treatment regimes under endogeneity,” *Journal of the American Statistical Association*, 116(533), 162–173.
- Groenwold, R. H. (2020), “Informative missingness in electronic health record systems: the curse of knowing,” *Diagnostic and prognostic research*, 4(1), 1–6.
- Hahn, P. R., Murray, J. S., and Carvalho, C. M. (2020), “Bayesian regression tree models for causal inference: Regularization, confounding, and heterogeneous effects (with discussion),” *Bayesian Analysis*, 15(3), 965–1056.

- He, D., Zhang, L., Hu, H., Gu, W.-j., Lu, X., Qiu, M., Li, C., Yin, H., and Lyu, J. (2023), “Effect of early vasopressin combined with norepinephrine on short-term mortality in septic shock: A retrospective study based on the MIMIC-IV database,” *The American Journal of Emergency Medicine*, 69, 188–194.
- Hou, N., Li, M., He, L., Xie, B., Wang, L., Zhang, R., Yu, Y., Sun, X., Pan, Z., and Wang, K. (2020), “Predicting 30-days mortality for MIMIC-III patients with sepsis-3: a machine learning approach using XGboost,” *Journal of translational medicine*, 18(1), 1–14.
- Hu, J., Lv, C., Hu, X., and Liu, J. (2021), “Effect of hypoproteinemia on the mortality of sepsis patients in the ICU: a retrospective cohort study,” *Scientific Reports*, 11(1), 24379.
- James, N. D., Sydes, M. R., Clarke, N. W., Mason, M. D., Dearnaley, D. P., Spears, M. R., Ritchie, A. W., Parker, C. C., Russell, J. M., Attard, G., de Bono, J., Cross, W., Jones, R. J., Thalmann, G., Attard, G., de Bono, J., Cross, W., Jones, R. J., Thalmann, G., Atmos, C., Matheson, D., Millman, R., Alzouebi, M., Beesley, S., Birtle, A., Brock, S., Cathomas, R., Chakraborti, P., Chowdhury, S., Cook, A., Elliott, T., Gale, J., Gibbs, S., Graham, J. D., Hetherington, J., Hughes, R., Laing, R., McKinna, F., McLaren, D. B., O’Sullivan, J. M., Parikh, O., Peedell, C., Protheroe, A., Robinson, A. J., Srihari, N., Srinivasan, R., Staffurth, J., Sundar, S., Tolan, S., Tsang, D., Wagstaff, J., Parmar, M. K. B., and investigators, S. (2016), “Addition of docetaxel, zoledronic acid, or both to first-line long-term hormone therapy in prostate cancer (STAMPEDE): survival results from an adaptive, multiarm, multistage, platform randomised controlled trial,” *The Lancet*, 387(10024), 1163–1177.
- Jazayeri, A., Liang, O. S., and Yang, C. C. (2020), “Imputation of missing data in electronic health records based on patients’ similarities,” *Journal of Healthcare Informatics Research*, 4, 295–307.
- Jiang, R., Lu, W., Song, R., and Davidian, M. (2017), “On estimation of optimal treatment regimes for maximizing t-year survival probability,” *Journal of the Royal Statistical Society Series B: Statistical Methodology*, 79(4), 1165–1185.
- Jing, L., Ng, M. K., and Huang, J. Z. (2007), “An Entropy Weighting k -Means Algorithm for Subspace Clustering of High-Dimensional Sparse Data,” *IEEE Transactions on Knowledge and Data Engineering*, 19(8), 1026–1041.

- Johnson, A. E., Pollard, T. J., Shen, L., Lehman, L.-w. H., Feng, M., Ghassemi, M., Moody, B., Szolovits, P., Anthony Celi, L., and Mark, R. G. (2016), “MIMIC-III, a freely accessible critical care database,” *Scientific data*, 3(1), 1–9.
- Jones, P. H., Davidson, M. H., Stein, E. A., Bays, H. E., McKenney, J. M., Miller, E., Cain, V. A., Blasetto, J. W., and Group, S. S. (2003), “Comparison of the efficacy and safety of rosuvastatin versus atorvastatin, simvastatin, and pravastatin across doses (STELLAR Trial),” *The American journal of cardiology*, 92(2), 152–160.
- Karatzoglou, A., Smola, A., Hornik, K., and Zeileis, A. (2004), “kernlab – An S4 Package for Kernel Methods in R,” *Journal of Statistical Software*, 11(9), 1–20.
- Kenzaka, T., Okayama, M., Kuroki, S., Fukui, M., Yahata, S., Hayashi, H., Kitao, A., Sugiyama, D., Kajii, E., and Hashimoto, M. (2012), “Importance of vital signs to the early diagnosis and severity of sepsis: association between vital signs and sequential organ failure assessment score in patients with sepsis,” *Internal Medicine*, 51(8), 871–876.
- Khanna, A. K., Kinoshita, T., Natarajan, A., Schwager, E., Linn, D. D., Dong, J., Ghosh, E., Vicario, F., and Maheshwari, K. (2023), “Association of systolic, diastolic, mean, and pulse pressure with morbidity and mortality in septic ICU patients: a nationwide observational study,” *Annals of Intensive Care*, 13(1), 1–13.
- Künzel, S. R., Sekhon, J. S., Bickel, P. J., and Yu, B. (2019), “Metalearners for estimating heterogeneous treatment effects using machine learning,” *Proceedings of the National Academy of Sciences*, 116(10), 4156–4165.
- Kuo, L., and Mallick, B. (1998), “Variable selection for regression models,” *Sankhyā: The Indian Journal of Statistics, Series B*, pp. 65–81.
- Li, F., Ding, P., and Mealli, F. (2023), “Bayesian causal inference: a critical review,” *Philosophical Transactions of the Royal Society A*, 381(2247), 20220153.
- Li, F., Xin, H., Zhang, J., Fu, M., Zhou, J., and Lian, Z. (2021), “Prediction model of in-hospital mortality in intensive care unit patients with heart failure: machine learning-based, retrospective analysis of the MIMIC-III database,” *BMJ open*, 11(7), e044779.

- Li, Z., Chen, J., Laber, E., Liu, F., and Baumgartner, R. (2023), “Optimal treatment regimes: a review and empirical comparison,” *International Statistical Review*, .
- Linero, A. R., and Yang, Y. (2018), “Bayesian regression tree ensembles that adapt to smoothness and sparsity,” *Journal of the Royal Statistical Society: Series B (Statistical Methodology)*, 80(5), 1087–1110.
- Luedtke, A. R., and Van Der Laan, M. J. (2016), “Statistical inference for the mean outcome under a possibly non-unique optimal treatment strategy,” *Annals of statistics*, 44(2), 713.
- McCaffrey, D. F., Griffin, B. A., Almirall, D., Slaughter, M. E., Ramchand, R., and Burgette, L. F. (2013), “A tutorial on propensity score estimation for multiple treatments using generalized boosted models,” *Statistics in medicine*, 32(19), 3388–3414.
- McCulloch, R., Sparapani, R., Gramacy, R., Spanbauer, C., and Pratola, M. (2019), *BART: Bayesian Additive Regression Trees*. R package version 2.7.
- Meyer, D., Dimitriadou, E., Hornik, K., Weingessel, A., and Leisch, F. (2019), *e1071: Misc Functions of the Department of Statistics, Probability Theory Group (Formerly: E1071), TU Wien*. R package version 1.7-3.
- Nie, X., and Wager, S. (2021), “Quasi-oracle estimation of heterogeneous treatment effects,” *Biometrika*, 108(2), 299–319.
- Peine, A., Hallawa, A., Bickenbach, J., Dartmann, G., Fazlic, L. B., Schmeink, A., Ascheid, G., Thiemermann, C., Schuppert, A., Kindle, R., Celi, L., Marx, G., and Martin, L. (2021), “Development and validation of a reinforcement learning algorithm to dynamically optimize mechanical ventilation in critical care,” *NPJ digital medicine*, 4(1), 32.
- Rekkas, A., Paulus, J. K., Raman, G., Wong, J. B., Steyerberg, E. W., Rijnbeek, P. R., Kent, D. M., and van Klaveren, D. (2020), “Predictive approaches to heterogeneous treatment effects: a scoping review,” *BMC Medical Research Methodology*, 20(1), 1–12.
- Roy, A. (2023), “Nonparametric group variable selection with multivariate response for connectome-based modelling of cognitive scores,” *Journal of the Royal Statistical Society Series C: Applied Statistics*, 72(4), 872–888.

- Sarkar, S., Singh, S., and Rout, A. (2022), “Mean arterial pressure goal in critically ill patients: a meta-analysis of randomized controlled trials,” *Journal of Clinical Medicine Research*, 14(5), 196.
- Semenova, V., and Chernozhukov, V. (2021), “Debiased machine learning of conditional average treatment effects and other causal functions,” *The Econometrics Journal*, 24(2), 264–289.
- Singer, M., Deutschman, C. S., Seymour, C. W., Shankar-Hari, M., Annane, D., Bauer, M., Bellomo, R., Bernard, G. R., Chiche, J.-D., Coopersmith, C. M., Hotchkiss, R. S., Levy, M. M., Marshall, J. C., Martin, G. S., Opal, S. M., Rubenfeld, G. D., van der Poll, T., Vincent, J.-L., and Angus, D. C. (2016), “The third international consensus definitions for sepsis and septic shock (Sepsis-3),” *Jama*, 315(8), 801–810.
- Taddy, M., Gardner, M., Chen, L., and Draper, D. (2016), “A nonparametric bayesian analysis of heterogenous treatment effects in digital experimentation,” *Journal of Business & Economic Statistics*, 34(4), 661–672.
- Tibshirani, J., Athey, S., Sverdrup, E., and Wager, S. (2023), *grf: Generalized Random Forests*. R package version 2.3.0.
URL: <https://CRAN.R-project.org/package=grf>
- Ursprung, S., Mossop, H., Gallagher, F. A., Sala, E., Skells, R., Sipple, J. A., Mitchell, T. J., Chhabra, A., Fife, K., Matakidou, A., Young, G., Walker, A., Thomas, M. G., Ortuzar, M. C., Sullivan, M., Protheroe, A., Oades, G., Venugopal, B., Warren, A. Y., Stone, J., Eisen, T., Wason, J., Welsh, S. J., and Stewart, G. D. (2021), “The WIRE study a phase II, multi-arm, multi-centre, non-randomised window-of-opportunity clinical trial platform using a Bayesian adaptive design for proof-of-mechanism of novel treatment strategies in operable renal cell cancer—a study protocol,” *BMC cancer*, 21, 1–11.
- van Buuren, S., and Groothuis-Oudshoorn, K. (2011), “mice: Multivariate Imputation by Chained Equations in R,” *Journal of Statistical Software*, 45(3), 1–67.
- Van Der Laan, M. J., and Rubin, D. (2006), “Targeted maximum likelihood learning,” *The International Journal of Biostatistics*, 2(1).

- Wager, S., and Athey, S. (2018), “Estimation and inference of heterogeneous treatment effects using random forests,” *Journal of the American Statistical Association*, 113(523), 1228–1242.
- Wendling, T., Jung, K., Callahan, A., Schuler, A., Shah, N. H., and Gallego, B. (2018), “Comparing methods for estimation of heterogeneous treatment effects using observational data from health care databases,” *Statistics in medicine*, 37(23), 3309–3324.
- White, W. B., Weber, M. A., Sica, D., Bakris, G. L., Perez, A., Cao, C., and Kupfer, S. (2011), “Effects of the angiotensin receptor blocker azilsartan medoxomil versus olmesartan and valsartan on ambulatory and clinic blood pressure in patients with stages 1 and 2 hypertension,” *Hypertension*, 57(3), 413–420.
- Williams, G., Huang, J. Z., Chen, X., Wang, Q., and Xiao, L. (2020), *wskm: Weighted k-Means Clustering*. R package version 1.4.40.
URL: <https://CRAN.R-project.org/package=wskm>
- Xu, J., Cai, H., and Zheng, X. (2023), “Timing of vasopressin initiation and mortality in patients with septic shock: analysis of the MIMIC-III and MIMIC-IV databases,” *BMC Infectious Diseases*, 23(1), 1–10.
- Xue, J., and Liang, F. (2017), “A robust model-free feature screening method for ultrahigh-dimensional data,” *Journal of Computational and Graphical Statistics*, 26(4), 803–813.
- Zeileis, A., and Grothendieck, G. (2005), “zoo: S3 Infrastructure for Regular and Irregular Time Series,” *Journal of Statistical Software*, 14(6), 1–27.
- Zhang, B., Tsiatis, A. A., Laber, E. B., and Davidian, M. (2012), “A robust method for estimating optimal treatment regimes,” *Biometrics*, 68(4), 1010–1018.
- Zhu, Y., Zhang, J., Wang, G., Yao, R., Ren, C., Chen, G., Jin, X., Guo, J., Liu, S., Zheng, H., Chen, Y., Guo, Q., Li, L., Du, B., Xi, X., Li, W., Huang, H., Li, Y., and Yu, Q. (2021), “Machine learning prediction models for mechanically ventilated patients: analyses of the MIMIC-III database,” *Frontiers in medicine*, 8, 662340.